MODIFICATION OF SILICON MICROSEGREGATION IN SOLID-SOLUTION-STRENGTHENED DUCTILE IRON BY ALLOYING WITH ALUMINUM

D. Franzen, P. Weiß, B. Pustal, and A. Bührig-Polaczek
Foundry-Institute RWTH Aachen, Aachen, Germany

Abstract

In solid-solution-strengthened ferritic ductile iron (SSFDI), a silicon content above 4.3 wt% leads to an abrupt decrease in ultimate tensile strength and elongation at fracture. This phenomenon has recently been proven to be attributed to the formation of iron–silicon long-range orderings that lead to an embrittlement of the material. It is assumed that the local tendency to form silicon superstructures is promoted in particular by the occurrence of silicon microsegregation. During solidification of ductile iron, silicon segregates inversely into the austenite. Thus, the highest silicon concentration is larger than the initial concentration of the melt and is located directly at the graphite nodules. As a straight consequence, the presence of silicon superstructures is expected primarily in these areas. Therefore, the focus is on homogenization of the silicon microsegregation profile in order to avoid the formation of brittle iron–silicon superstructures. For this purpose, in the present study the alloying concept of SSFDI is adapted. Thermodynamic–kinetic simulations as well as experimental investigations indicate that aluminum concentrations of approx. 1.2 wt% lead to an inversion of the silicon microsegregation. The findings provide a promising tool to shift the silicon embrittlement in SSFDI to higher silicon concentrations. This method could be used to increase the maximum strength, to improve toughness properties or to increase the process integrity against deviations in silicon content.

Keywords: solid solution strengthening, ductile iron, spheroidal graphite cast iron, silicon, aluminum, long-range ordering, superstructure, microsegregation

Introduction

The possibility of strengthening the matrix in ductile iron by increased silicon contents producing a solid-solution-strengthened ductile iron was rejected for a long time. However, in the 1950s and 1960s, White et al. were able to demonstrate that increased silicon contents of about 4 to 5 wt% lead to the effect of solid solution strengthening, which made it possible to achieve high strengths with very good elongations at fracture at the same time. Due to the fully ferritic metal matrix, improved machinability was predicted in comparison with conventional, ferritic–pearlitic grades of spheroidal graphite iron (SGI).[1] A few decades later, the subject of silicon-strengthened SGI cast iron materials was taken up again. In the mid 1990s, Björkegren et al. conducted experiments on solid solution strengthening of SGI with the aim of reducing hardness scattering in ferritic–pearlitic ductile iron grades. Machinability could significantly be improved by adjusting a purely ferritic matrix due to a more homogeneous hardness distribution with very good tensile strengths and elongations, which led to cost savings of about 10% in mechanical machining.[2,3] As a result, grades of solid-solution-strengthened SGI materials were incorporated into the Swedish standards SS 140720 and SS 140725 in 1998 due to their extremely advantageous static mechanical properties. Further investigations in the following years proved the suitability of increased silicon contents for setting an advantageous ratio of tensile strength and elongation at fracture.[4,5] In their studies, particularly, materials with minimum values of ultimate tensile strength of 520 MPa and elongation at fracture of 14% were successfully adjusted. In 2012, the solid-solution-strengthened grades

EN-GJS-450-18 with 3.2 wt% Si, EN-GJS-500-14 with 3.8 wt% Si and EN-GJS-600-10 with 4.3 wt% Si were incorporated into the European standard DIN EN 1563.[6] This development has led to a significant increase in industrial applications in recent years, such as the automotive industry, maritime industry, wind power technology and mechanical engineering.[7–10]

In addition to the advantages of alloying with silicon, however, also some issues occur. It was shown that the maximum amount of silicon is limited to 4.3 wt%.[11] Above these contents, mechanical properties rapidly decrease. In particular, the elongation at fracture drops to almost 0% for contents greater than 4.3 wt% Si. Furthermore, increased silicon contents are accompanied by significantly lower Charpy impact toughness values. By increasing the silicon content from about 2.4 wt% Si in a ferritic–pearlitic EN-GJS-400-15 to about 3.8 wt% Si in the solid-solution-strengthened grade GJS-500-14, the transition temperature from ductile to brittle fracture is reduced by up to 70 °C, according to Figure 1.[12] Previous publications aimed to optimize the toughness properties of solid-solution-strengthened materials on a global level by adapting the alloying concept. In this context, improved Charpy impact values could be obtained by selectively adjusting the contents of the elements nickel and aluminum.[13,14] However, no further studies are known concerning further improvement in the toughness properties on a microstructural level.

The abrupt decrease in static and dynamic mechanical properties that was mentioned above is currently attributed to the formation of iron–silicon long-range orderings that are known from high-silicon steels.[15,16] These iron–silicon superstructures, which occur as B2- and DO_3-ordered phases (Figure 2 [17]), are assumed to be the root cause of embrittlement occurring at elevated silicon contents. Analyses in previous publications have proven the formation of superstructures in samples with increased levels of silicon using transmission electron microscopy. Samples with a silicon content of 5.36 wt% showed significant B2- and DO_3-superstructures reflections. Reflections of B2-superstructures could also be detected in samples with 3.95 wt% Si. Thus, it can be assumed that the effect of embrittlement of the material is to be expected even at silicon levels below the critical limit of 4.3 wt% Si.[18]

The decoupled eutectic solidification of ductile iron alloys due to the formation of a closed austenite halo around the precipitating graphite nodules in particular causes the formation of distinct microsegregation profiles in ductile iron microstructures. While negative segregating elements such as silicon and aluminum accumulate in the solidifying austenitic crystal lattice, elements such as manganese and chromium are rejected at the solid–liquid interface and thus enriching in the last-to-freeze zones tending to stabilize carbides. In 1996, S. Hasse assigned segregation factors to several alloying elements in spheroidal graphite iron that allow a qualitative estimation of the intensity of microsegregations.[19]

In order to reduce the formation of iron–silicon superstructures and thus to further develop the mechanical properties of high silicon ductile iron grades, approaches have been taken in the past to homogenize the microsegregations by suitable heat treatments. However, own unpublished preliminary investigations show that annealing times of 24 h at about 975 °C do not significantly influence the microsegregation profile of silicon. It is therefore assumed that the effect of heat treatments on the silicon microsegregation profile is very time and cost-intensive and thus represents an uneconomical possibility to modify the silicon segregation profile in SGI.

So far, however, there have been no studies on influencing the silicon microsegregation profile on a microstructural and local level by adapting the alloy concept. Therefore, current investigations are pursuing metallurgical approaches to further develop the mechanical properties by modifying the microstructure, in particular the silicon microsegregation profile. In order to close this current research gap, the influence of aluminum on the silicon microsegregation in SSFDI was analyzed on numerical and experimental bases.

Design of Experiments

In order to determine the effect of aluminum on the microsegregation of silicon, different investigations were carried out on both numerical and experimental bases. Numerical investigations were conducted in order to predict the formation of silicon microsegregation profiles for different aluminum contents of 0 and 1.2 wt% Al. To verify the prediction on an experimental basis and to investigate the effect of aluminum on the microsegregation of silicon
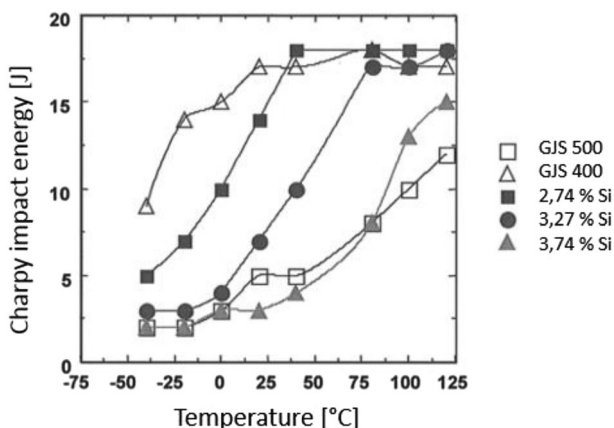
Figure 1. Charpy impact energy as a function of temperature for different SGI materials is shown, accord. to Reference 12.
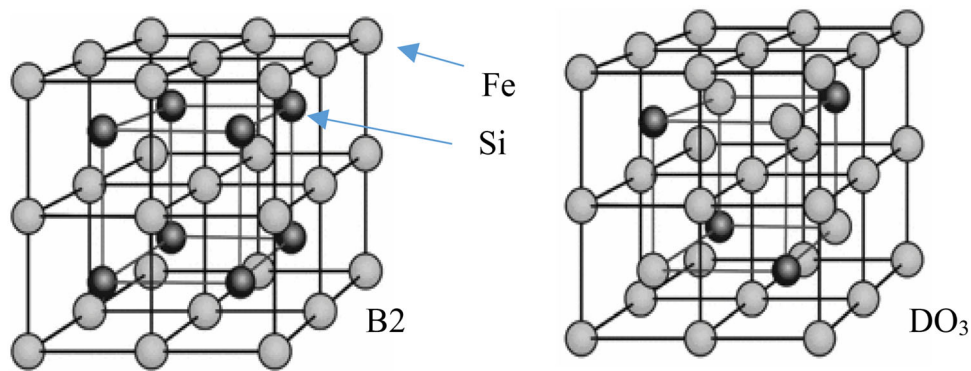
Figure 2. *Iron–silicon B2 and DO$_3$ long-range orderings are shown, accord. to Reference 17.*

qualitatively and quantitatively, a series of six alloys, referred to as alloy 1–6, with a silicon content of 3.8 wt% and an aluminum content of 0 and 1.2 wt% was produced and investigated. As a reference alloy without aluminum, alloy 1 corresponds to an EN-GJS-500-14 according to the European standard DIN EN 1563.[6] Alloys 2–6 are each adjusted with an aluminum content of 1.2 wt% Al in order to produce a sufficient amount of samples.

Experimental Procedure

Raw materials (recirculation material, pure iron and ferrosilicon (FeSi)) were prepared and melted in a 50-kg medium-frequency induction furnace using a graphite crucible. After melting all raw materials, at 1400 °C solid pieces of Al 99.8 were immersed into the melt using a plunger. The melt was reheated to 1400 °C, and spectrometer samples were produced to evaluate the adjusted aluminum content. This is followed by overheating to 1500 °C and holding this temperature for about five minutes in order to remove impurities from the melt. After deslagging the melt, magnesium treatment with a magnesium master alloy containing cerium at about 1380 °C was performed using a plunger. After the melt was deslagged, the inoculation was carried out by adding 0.3 wt% of a bismuth- and cerium-based inoculant. Samples for thermal analyses as well as spectrometrical analyses were produced, and the melt was cast at 1350 °C. Additional external wet-chemical analyses were conducted in order to verify the aluminum content in the alloys. For each casting, one furan-bounded sand mold, containing one Y2 (module: 0.8 cm), one Y4 (module: 1.7 cm) standard test blocks, and one insulated cylindrical sample with a diameter of 130 mm (module: 3.0 cm) are produced. For each casting, five tensile test specimens are machined from the positions marked in Figure 3. Samples for both metallographic and electron microscopic examinations are machined from the direct vicinity of the tensile test specimens.
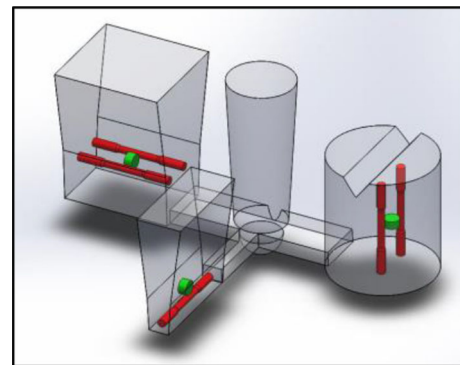

Figure 3. *Each casting contains specimens for tensile tests, metallographic and electron microscopic examinations.*

Simulation Procedure

The aim of the material simulation performed is to simulate the solidification kinetics along with the microsegregation patterns in the austenite. For this purpose, the microsegregation model [20] was used along with thermodynamic (TCFE6) and mobility data (MOBFE2). The coupling to thermodynamic and kinetic information is realized by applying the tq-library of Thermo-Calc. The thermodynamic data are required to obtain the boundary conditions at the graphite–austenite and the austenite–liquid interfaces in order to simulate diffusion in the austenite. This allows predicting the transformation kinetics. In particular, the diffusion of carbon from the liquid through the austenite to the graphite nodule is important. In this diffusion simulation, also cross-effects between the gradients of other alloying elements are taken into account. One example is the diffusion of carbon in the gradients of Si, Al, and Mn. Initially, a liquid melt at 1500 °C and a composition of FeSi3.8C are cooled down by a heat extraction rate of 650 W/kg. The representative volume element is considered to be spherical with a radius of 42 μm. These conditions correspond to the experimental cooling conditions and the nodule count in the Y4 standard test block.

Specimen Analyses

Mechanical Properties

A total of five tensile test samples are produced as indicated in Figure 3 for mechanical testing of the alloys. Cylindrical samples with a diameter of 18 mm are taken from the castings using a water-cooled core drill. The position of the samples in the Y2-and Y4-test block geometry corresponds to the positions A and A, C from the DIN EN 1563 standard, respectively. From these, tensile test specimens of shape A are machined, according to DIN EN 50125, with a diameter of 8 mm and an overall length of 115 mm. In order to determine mechanical properties, tensile tests are conducted using a main cross-speed of 0.60 mm/min.

Metallographic Examinations

Samples for metallographic examinations are taken from the direct vicinity of the tensile test specimen. Using a water-cooled saw, metallographic samples with a thickness of about 2 cm are separated from the castings. The metallographic samples are embedded and then subjected to four successive grinding processes with grain sizes 180, 320, 500, 1000 for 2 min each at a contact pressure of 20 N and 150 rates per minute with water as lubricant. The samples are then each polished on three polishing stages with diamond suspensions of grain sizes 9 μm, 3 μm and 0.25 μm at a pressure of 25 N for 3–4 min. Etchings according to Klemm [21] are performed in order to visualize silicon microsegregation profiles by metallographic examinations. Microstructural analyses of both polished and etched specimens are carried out using an optical up-light microscope.

Chemical Composition

Spectrometer samples are produced pouring the melt in a copper die after alloying with aluminum and investigated using a spark emission spectrometer after grinding with coarse SiC-grinding paper. Single aluminum contents are tested by wet-chemical examination methods. The chemical compositions of the produced melts can be obtained from Table 1. Whereas some deviations in the setting of the silicon content can be observed, the aluminum content of 1.2 wt% could be adjusted very reproducibly. Carbon equivalent is calculated using Eqn. 1:

$$CE = \%C + \frac{\%Si}{3} + \frac{\%Al}{8} \qquad \text{Eqn. 1}$$

Results

Figure 4 shows the mechanical properties determined from Y2 standard test blocks comparing the six samples. Without aluminum, the ultimate tensile strength (UTS) is 560 MPa and the yield strength (YS) 436 MPa at an elongation (A) of 22.4%. By alloying with about 1.2 wt% Al, a significant increase in ultimate tensile strength of about 50 MPa and an increase in yield strength of about 80 MPa could be achieved. At the same time, the elongation is decreasing rapidly to about 9%, which is suggested to be due to the negative influence of aluminum on the graphite growth, resulting in the formation of compacted graphite. The negative effect on the graphite morphology is shown in Figure 5. Whereas samples from Y2 standard test blocks containing no aluminum have an average nodularity of about 80%, the nodularity in samples containing 1.2 wt% Al is only about 74% at comparable residual magnesium contents. At the same time, the nodule count is increased from 154 to 192 $1/mm^2$ by the addition of aluminum. Deep etchings are performed in order to visualize the graphite morphology in three dimensions. In samples alloyed with aluminum, graphite precipitates were classified as compacted graphite, as shown in Figure 6 as example. As can be seen from Figure 6, the number of nodules increases considerably in alloys with aluminum addition. A number of larger graphite precipitates with particularly low nodularity and an increased number of

Table 1. Spectrometer and Wet-Chemical Analyses (*) of the Six Melts That Were Investigated

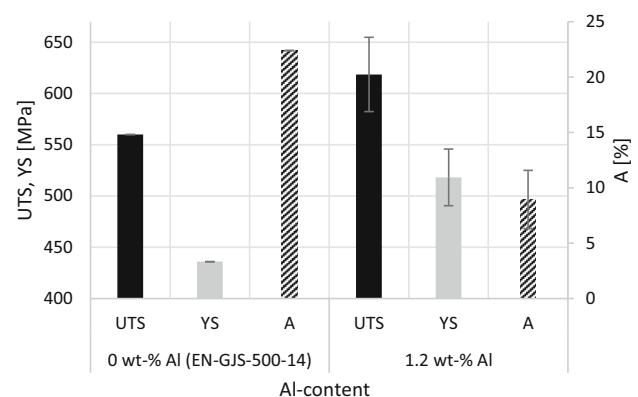| Alloy	C-content (wt%)	Si-content (wt%)	Al-content (wt%)	Mg-content (wt%)	CE
1	2.91	4.03	0.01	0.038	4.25
2	2.91	3.86	1.17*	0.048	4.33
3	2.75	3.77	1.17	0.044	4.15
4	2.67	4.04	1.11	0.068	4.15
5	2.68	3.81	1.21*	0.024	4.10
6	2.72	4.13	1.19	0.041	4.24

Figure 4. Ultimate tensile strength (UTS), yield strength (YS) and elongation at fracture (A) are measured in Y2 standard test blocks for alloys with 0 wt% and 1.2 wt% Al.
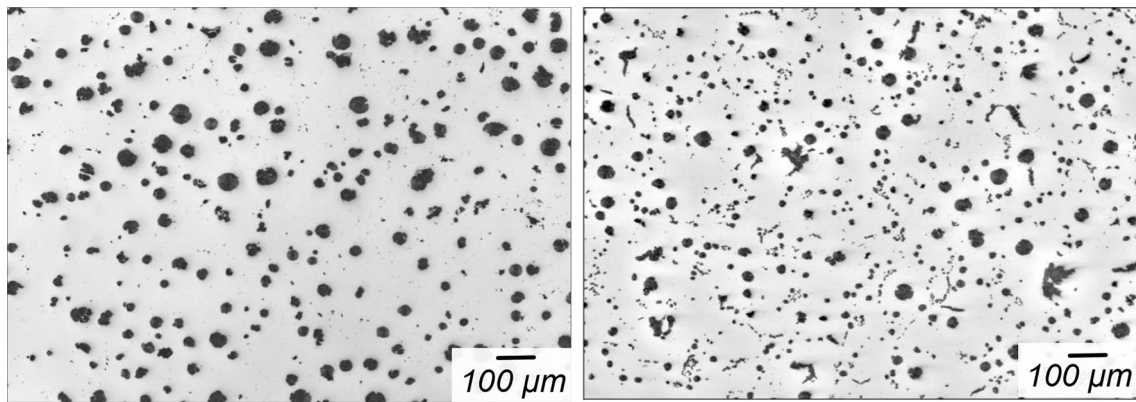
Figure 5. Microstructure in samples from Y2 standard test blocks is analyzed by image analyses (left 0 wt% Al, 0.039 wt% Mg, 80.1% nodularity; right 1.17 wt% Al, 0.042 wt% Mg, 74.2% nodularity).
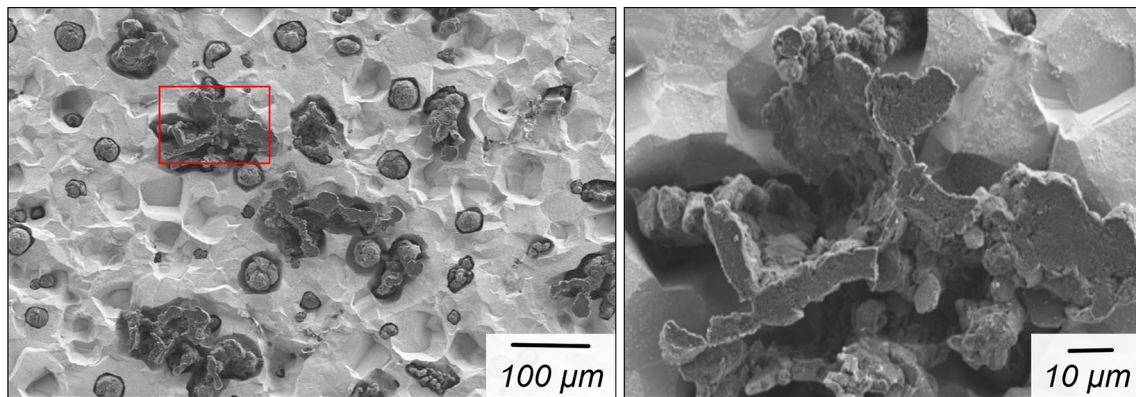

Figure 6. Deep-etching of a sample with 1.12 wt% Al is conducted in order to investigate the 3D-graphite morphology.
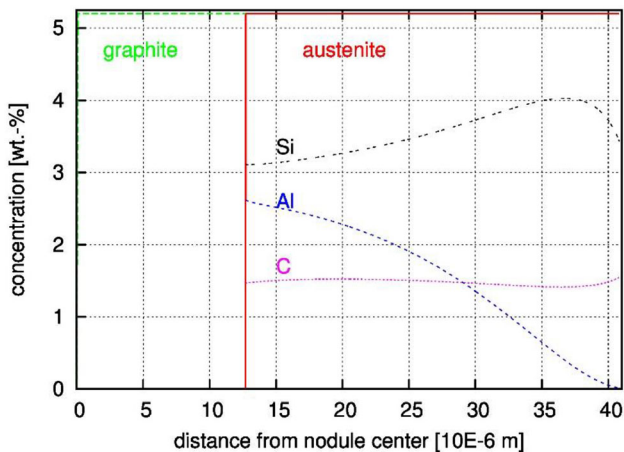

Figure 7. Microsegregation profiles were determined for the elements aluminum, carbon and silicon at the end of eutectic solidification at 1138 °C along the radius of a eutectic grain.

smaller graphite spheres with higher roundness can be observed from metallographic analyses.

For the eutectic solidification at a temperature of 1138 °C, Figure 7 shows as one simulation result the microsegregation profiles of the main elements in the alloy FeCSi3.8Al1.2Mn0.1 along the radius of the eutectic grain. Carbon shows no significant gradient. However, in order to allow for a decoupled eutectic solidification carbon has to diffuse through the austenite halo. This is possible because Si and Al have a large impact on the activity of C. Thus, carbon diffuses in the gradient of Si and Al. Nevertheless, both elements reduce the speed of diffusion and therefore also the transformation kinetics. This negative interaction effect is also known from the segregation of C in gradients of nickel where it leads to chunky graphite.[22] Chunky graphite and reduced nodularity were also found in the five samples alloyed with Al (c.f. Figure 5). Besides, a significant depletion of aluminum and a strong positive segregation of silicon are predicted in the last solidifying areas. With a global aluminum content of 1.2 wt% Al, about 2.6 wt% Al are predicted directly at the graphite–austenite interface, while the concentration at a distance of 42 μm is close to zero. The silicon concentration increases from 3.1 wt% up to approx. 4.1 wt% Si in the last-to-freeze areas.

In order to investigate the microsegregation profiles of silicon and aluminum that are predicted by the model, metallographic investigations are carried out with the aim of qualitatively visualizing the microsegregation behavior.

Two samples with 0 wt% and 1.17 wt% Al are subjected to Klemm etchings and compared using light-optical analyses (according to Figure 8). Brown-to-light-yellow areas indicate increased silicon contents, while blueish zones indicate silicon depletion. In the sample without aluminum, areas near the graphite nodules appear light yellow, while blue coloration can be observed in the last solidifying zones. A contrasting pattern can be seen in the analyses of samples with 1.17 wt% Al. In these, areas in direct vicinity to the graphite nodules appear blue, indicating silicon depletion. However, zones that tend to be assigned as last-to-freeze areas appear in a brownish color.

To validate the results using electron microscopic analyses, element mappings are performed using energy-dispersive X-ray spectroscopy (EDX) and element line scans of the silicon and aluminum concentration gradients. Figure 9 shows the distribution of the elements silicon (a) and aluminum (b) in a specimen with the chemical composition 2.75 wt% C, 3.77 wt% Si and 1.17 wt% Al. With regard to the distribution of the silicon concentration, no definite

findings can be provided. However, discernible distinctions of the aluminum concentration can be qualitatively observed in coloring (b). Bright areas can be found in areas near the graphite nodules, indicating an enrichment of aluminum in these zones. On the other hand, darkly colored and thus zones with lower aluminum concentrations are located between individual graphite nodules, tending to be the last-to-freeze areas.

Figure 10a shows the area that was investigated by means of EDX line scans. Linking to this, the formation of silicon and aluminum microsegregation profiles in a specimen with 1.17 wt% Al is presented in Figure 10b. Due to the presence of chunky graphite and several precipitates in the central region of the image shown as follows, this zone could be clearly identified as a last-to-freeze area. A total of 12 measuring points were investigated in order to compare the results with the microsegregations predicted by numerical simulation. It can be observed that the minimum silicon content is approx. 4.0 wt% in vicinity of the graphite nodule and increases up to 4.55 wt% Si with
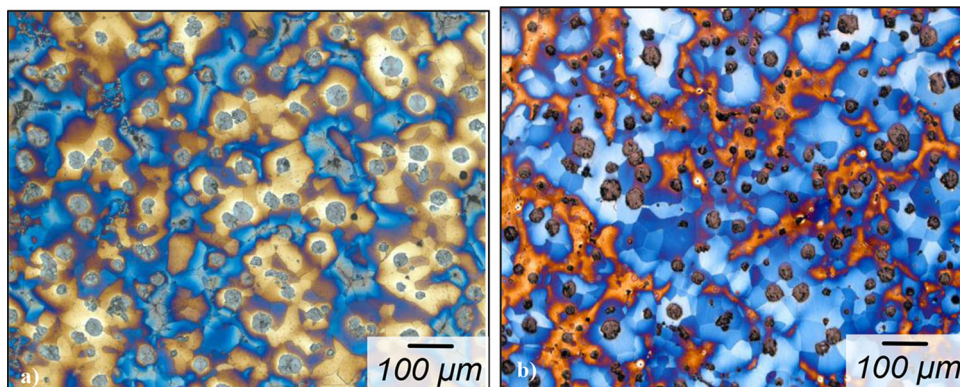

Figure 8. Klemm etchings on Y4 samples at magnification for specimen with (a) 4.02 wt% Si and 0.01 wt% Al (alloy 1) and (b) 3.86 wt% Si and 1.17 wt% Al (alloy 2) are conducted.
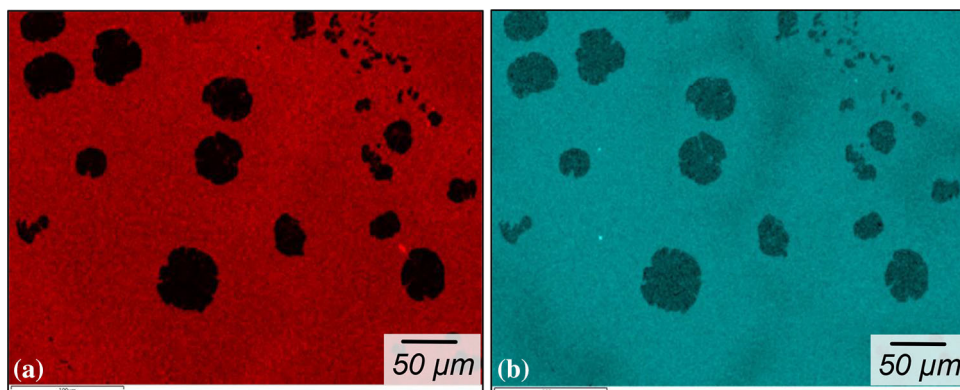

Figure 9. The concentration gradients of Si and Al in a specimen with 2.75 wt% C, 3.77 wt% Si and 1.17 wt% Al (alloy 3) are measured by EDX-mappings: (a) silicon and (b) aluminum.
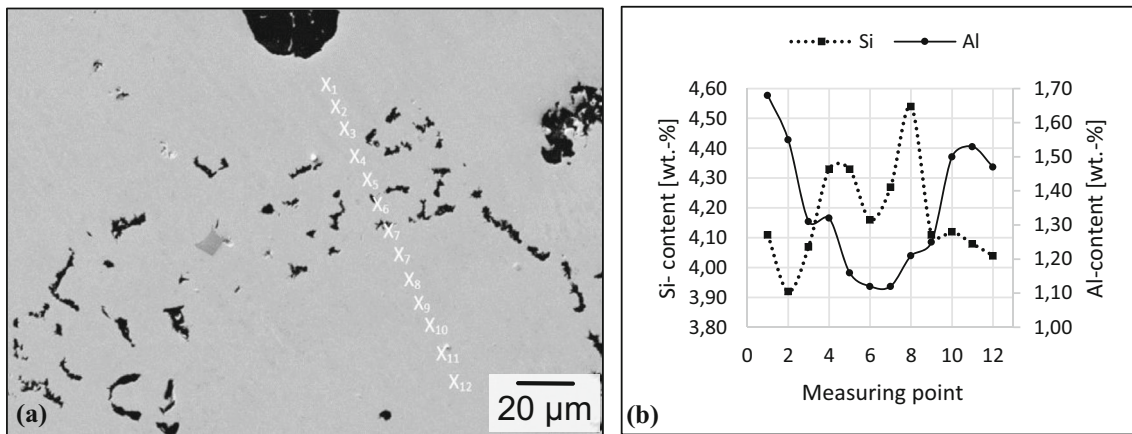
Figure 10. EDX line scans in a specimen with 2.75 wt% C, 3.77 wt% Si and 1.17 wt% Al (alloy 3) are conducted.

increasing distance from the graphite nodule. In contrast, a negative and thus an inverted microsegregation profile of aluminum from the graphite nodule to the last-to-freeze area can be observed. The aluminum content decreases from almost 1.7 wt% Al at the graphite sphere down to about 1.1 wt% Al. Additional EDX line scans that were conducted on further castings show similar results.

Discussion

By alloying the ductile iron grade EN-GJS-500-14 (accord. to the European standard DIN EN 1563), with 1.2 wt% Al, a significant increase in ultimate tensile strength from 560 MPa to 618 MPa and in yield strength from 436 MPa to about 520 MPa can be achieved. Analogous to the element silicon, aluminum is preferably dissolved in the austenite crystal lattice during eutectic solidification, which leads to a strengthening of the metallic matrix resulting in a higher ultimate tensile strength. Compared to the effect of silicon, alloying with aluminum causes much higher increase in yield strength. Consequently, the UTS/YS ratio is increased from 0.78 to 0.83, which means, on the one hand, enhancement of the useable material strength. On the other hand, however, this improvement is associated with a rapid decrease in elongation from 22.4% to about 9%. As a result, an elongation of 14%, that is required in the standard for a GJS-500-14 in this wall thickness, is not met. Due to the negative effect on the graphite morphology in ductile cast iron that is known from the literature,[23–25] alloying with aluminum is attributed to an increased tendency to form compacted graphite. The negative effect of alloying with aluminum on the graphite morphology is particularly evident in a significant reduction in nodularity. While samples from Y2 test blocks containing no aluminum show an average nodularity of about 80%, the nodularity in samples containing 1.2 wt% Al is only about 74%. As a result, the specifications of a GJS-500-14 are not met. It is assumed that the global aluminum addition is limited to contents lower than 1 wt% Al due to the negative effect on

the graphite morphology. Compared to conventional ductile cast iron materials, the nodularity is reduced, which is attributed to higher silicon contents that are known to have a decreasing effect on the nodularity as well. Deviations in the mechanical properties that can be observed are assumed to be due to varying silicon contents that significantly determine the degree of solid solution strengthening of the alloys.

In the present investigations, a distinct interaction of the microsegregation profiles of aluminum and silicon could be demonstrated on both numerical and experimental bases. Using the microsegregation model, it could be shown that aluminum is preferably embedded into the solid solution resulting in a negative microsegregation profile of Al. In alloys with 3.8 wt% Si and 1.2 wt% Al, however, the model predicts a positive microsegregation profile of silicon, which is in contrast to the literature.[19,26,27] Nevertheless, these observations are confirmed by experimental work presented. Both metallographic and electron microscopic analyses show a clear correspondence. Based on the microsegregation profiles measured, a difference between the minimum and maximum contents of 0.8 wt% in the simulations and 0.7 wt% in the electron microscopic investigations can be determined for silicon. The segregation factors also calculated from this data representing the intensity of microsegregations are on average about 1.2. Thus, the degree of microsegregation is in accordance with literature data.[19] However, an analogous quantitative correlation cannot be determined for the microsegregation profiles of aluminum. The etchings carried out clearly show that silicon with the addition of 1.17 wt% Al is accumulated in zones that are to be identified as last-to-freeze areas, resulting in a positive microsegregation profile and favoring the formation of iron–silicon long-range orderings in these zones. The observations made are consistent with analyses carried out by Shayesteh-Zeraati et al. on samples with lower silicon contents.[28] They detect maximum silicon contents of about 1.6 wt% in the last-to-freeze areas in

the range between two graphite nodules with 4.88 wt% Al and 1.22 wt% Si in the as-cast samples. In 2012, Haghdadi et al. carry out similar tests on samples containing 6.16 wt% Al and 1.25 wt% Si and detect an enrichment of silicon of about 2.9 wt% in this range as well.[29] The increased silicon contents of 3.8 wt% Si that was set in the present work can be compared with the work of Muhmond et al., who produced samples with 3.16 wt% Al and 4.36 wt% Si with the aim of investigating the influence of aluminum on graphite morphology. By means of metallographic examinations, they were able to identify enrichment of aluminum in areas close to the graphite nodules.[30]

With focus on alloy development of solid-solution-strengthened ductile cast iron, the present work provides an innovative approach by means of metallurgical treatment to further improve the mechanical properties of SSFDI that are considered to be detrimental at increased silicon contents. In the present investigation, it could be shown that an inversion of the silicon microsegregation profile can be achieved by alloying with about 1.2 wt% aluminum. As a result of the findings in the current investigations, it is concluded that not only an inversion, but rather a precise modification of the silicon microsegregation can be realized by metallurgical approaches. Hence, for the authors a homogenization of the silicon microsegregation profile seems to be conceivable by precisely adjusting aluminum contents lower than 1 wt% Al in the melt. Consequently, this allows the local silicon contents at the graphite nodules to be reduced, which means increased safety against the formation of embrittling silicon long-range orderings that were described above. In this way, it could be possible to increase the globally adjusted silicon content in solid-solution-strengthened grades of ductile iron without the formation of brittle phases in the vicinity of the graphite nodules. Consequently, there would be an increased potential for improving the static and dynamic mechanical properties such as tensile strength, elongation at fracture and toughness properties. The possibility of homogenizing the microsegregation profile of silicon by alloying with aluminum, and thereby increasing the associated tolerance of the global silicon content, subsequently represents an important aspect that will be studied in further investigations.

Additionally, the present observations offer the possibility of increasing the globally adjustable nickel content in solid-solution-solidified SGI, which is currently limited by the formation of pearlite. As mentioned in,[13] advantageous effects with regard to the toughness properties could be observed by alloying with the pearlite-stabilizing element nickel. A controlled homogenization of the silicon microsegregation profile would therefore lead to higher adjustable silicon contents and, due to the associated increased ferrite-stabilizing effect, to the possibility of alloying with increased nickel contents. This impact is enhanced by the ferrite-stabilizing effect of aluminum.

Parallel to these investigations, the influence of aluminum and silicon on the formation of Al- and Si–Al superstructures should be considered, as it can be assumed that brittle phases occur with further increased contents of these elements. As it is well known, also aluminum has a solid solution strengthening effect [14,23,31,32] which means that a balanced silicon microsegregation profile does not lead to a balanced strength profile. It would also be possible to calculate an elemental distribution that would be required to set a balanced strength profile and to adjust segregation profiles that are as close as possible to it.

As a further outlook, the controlled modification of the silicon microsegregation profile could have an effect on the microstructure of the nodular graphite cast iron. In extreme cases, in alloys with a moderate content of pearlite-stabilizing elements the formation of pearlitic regions near the graphite nodules could be adjusted selectively. Due to the significant lower silicon content in direct vicinity of the graphite nodules and increased silicon contents in the remaining melt areas, the formation of pearlitic regions in the areas near the grain boundaries is inhibited and could be promoted directly at the graphite nodules. Since the crack propagation in SGI usually takes place along the graphite nodules, deliberate stabilization of pearlitic zones near the graphite spheres offers the possibility of inhibiting the crack propagation in these areas by using pearlitic zones as barriers against the propagating crack. A positive effect on the toughness properties of solid solutions strengthened grades of ductile cast iron would be the result. It should also be taken into account that aluminum, analogous to silicon, has a graphitizing effect and thus counteracts the formation of pearlitic zones due to its enrichment in the first solidifying areas.

Conclusions

The results can be summarized as follows:

1. Alloying with aluminum leads to significant increase in the ultimate tensile strength and yield strength, which is due to the solid solution hardening effect of aluminum. At the same time, the elongation at fracture is rapidly reduced to half of the initial values. The negative effect of aluminum on the graphite morphology, in particular the nodularity, is assumed to be the main cause for this observation. The authors therefore assume that an addition of aluminum is significantly limited to contents less than 1 wt% Al due to the negative effect of aluminum on the graphite morphology.
2. By alloying with aluminum, a distinct interaction with the silicon microsegregation profile can be observed. At a global silicon content of 3.8 wt% Si, aluminum contents of about 1.2 wt% Al lead

to an inversion of the silicon microsegregation resulting in silicon enrichment in the last-to-freeze areas. Both numerical by means of a numerical microsegregation model and experimental work in forms of metallographic and electron microscopic analyses confirm these findings.

Based on the results obtained from the present study, the following aspects are considered to be necessary to further investigate the effect of aluminum on silicon microsegregation in SSFDI:

3. It is assumed that it is possible to precisely modify the silicon microsegregation profile and thereby to homogenize the local strength gradient by alloying with aluminum.

4. With respect to the critical silicon causing the formation of brittle iron–silicon superstructures in the matrix, this opportunity is regarded to be a suitable metallurgical tool in order to increase the global silicon content without provoking a negative effect on the static and dynamic mechanical properties.

Acknowledgements

REFERENCES

1. W.H. White, L.P. Rice, A.R. Elsea, *Influence of Silicon Content on Mechanical and High-Temperature Properties of Nodular Cast Iron*. AFS Transactions, pp. 337–345 (1951)

2. L.-E. Björkegren, K. Hamberg, *Silicon Alloyed Ductile Iron with Excellent Ductility and Machinability*. Keith Millis Symposium on Ductile Cast Iron (2003)

3. L.-E. Björkegren, *Ferritic ductile iron with higher silicon content*. Swedish Foundry Association, 1994 (941028)

4. W. Kleinkröger, J. Stellmacher, D. Bounin, *Höherfeste GGG-Gussteile mit ausreichender Duktilität* (2001)

5. J. Kikkert, *Mischkristallverfestigtes ferritisches Gusseisen mit Kugelgraphit*. Deutscher Gießereitag 2009 – Tagungsband (2009)

6. DIN EN 1563: *Gießereiwesen – Gusseisen mit Kugelgraphit* (2012)

7. K. Vollrath, Neue, hochinteressante Kugelgraphit Gusswerkstoffe. Giesserei **100**, 70–73 (2013)

8. P. Mikoleizik, G. Geier, SiWind - Werkstoffentwicklung für Offshore-Windenergieanlagen im Multi-Megawatt-Bereich. Giesserei **9**(101), 64–69 (2014)

9. H. Werner, I. Lappat, B. Aurich, Mischkristallverfestigte EN-GJS-Werkstoffe für Groß- und Schwergussteile. Giesserei **103**(02), 38–42 (2016)

10. S. Seidel, Machbarkeitsstudie zur Herstellung von mischkristallverfetigtem ferritischem Gusseisen mit Kugelgrafit im Großguss Teil 1. Giesserei **103**(07), 24–27 (2016)

11. H. Löblich, *Schlussbericht AiF Vorhaben 41 EN: Werkstoff- und Fertigungstechnische Grundlagen der Herstellung und Anwendung von hoch Siliziumhaltigem Gusseisen mit Kugelgraphit* (2012)

12. L.E. Björkegren, K. Hamberg, B. Johannesson, Mechanische Eigenschaften von Silicium verfestigten ferritischen Gußeisen mit Kugelgraphit. Gießerei-Praxis **1**, 11–17 (1999)

13. P. Weiß, M. Riebisch, A. Bührig-Polaczek, Mechanical properties and impact toughness of nickel and aluminum alloyed high silicon ductile iron. Mater. Sci. Forum **925**, 304–310 (2018)

14. P. Weiß, *Schlussbericht zum IGF-Forschungsvorhaben 18554 N: Metallurgische Optimierung von hochsiliziumhaltigen mischkristallverfestigtem Gusseisen mit Kugelgraphit hinsichtlich der Sicherstellung der Zähigkeit und Prozessierbarkeit*. Aachen: 2017. 18554 N

15. B. Viala, J. Degauque, M. Fagot, M. Baricco, E. Ferrara, F. Fiorillo, Study of the brittle behaviour of annealed Fe-6.5 wt% Si ribbons produced by planar flow casting. Mater. Sci. Eng. A **212**(1), 62–68 (1996)

16. P.R. Swann, L. Grånäs, B. Lehtinen, The B2 and DO3 ordering reactions in iron-silicon alloys in the vicinity of the Curie temperature. Met. Sci. **9**(1), 90–96 (1975)

17. J.E. Wittig, G. Frommeyer, Deformation and fracture behavior of rapidly solidified and annealed iron-silicon alloys. Metall. Mater. Trans. A **39**(2), 252–265 (2008)

18. P. Weiß, A. Tekavcic, A. Bührig-Polaczek, Mechanistic approach to new design concepts for high

silicon ductile iron. Mater. Sci. Eng. A **713**, 67–74 (2018)

19. S. Hasse, *Duktiles Guseisen*, Edtion edn. (Schiele & Schön, Berlin, 1996)
20. B. Pustal, B. Böttger, A. Ludwig, P.R. Sahm, A. Bührig-Polaczek, Simulation of macroscopic solidification with an incorporated one-dimensional microsegregation model coupled to thermodynamic software. Metall. Mater. Trans. B **34**, 411–419 (2003)
21. H. Schumann, H. Oettel, *Metallografie*, Edtion edn. (Wiley-VCH Verlag, New York, 2011)
22. B. Pustal, A. Bührig-Polaczek, Physico-chemical causes of the formation of chunky graphite in austenitic ductile iron. Acta Mater. **124**, 137–142 (2017)
23. M.S. Soiński, A. Jakubus, P. Kordas, K. Skurka, Characteristics of graphite precipitates in aluminium cast iron treated with cerium mixture. Arch. Foundry Eng. **15**(1), 93–98 (2015)
24. M.S. Soiński, A. Jakubus, The influence of small amounts of aluminium on the effectiveness of cast iron spheroidization with magnesium. Arch. Fourndry Eng. **13**(3), 80–83 (2013)
25. K. Röhrig, H.-G. Gerlach, O. Nickel, *Legiertes Gusseisen – Band 2: Gusseisen mit Kugelgraphit*, Edtion edn. (Giesserei-Verlag GmbH, Düsseldorf, 1974)
26. G. Jolley, G. N. J. Gilbert. *Segregation in nodular iron and its influence on mechanical properties*. The British Foundryman (1967)
27. J. Lacaze, Solidification of spheroidal graphite cast irons: III. Microsegregation related effects. Acta Mater. **47**(14), 3779–3792 (1999)
28. A. Shayesteh-Zeraati, H. Naser-Zoshki, A.R. Kiani-Rashid, M.R. Yousef-Sani, The effect of aluminium content on morphology, size, volume fraction, and number of graphite nodules in ductile cast iron. Proc. Inst. Mech. Eng. Part L **224**, 117–122 (2010)
29. N. Haghdadi, B. Bazaz, H.R. Erfanian-Naziftoosi, A.R. Kiani-Rashid, Microstructural and mechanical characteristics of Al-alloyed ductile iron upon casting and annealing. Int. J. Miner. Metall. Mater. **19**(9), 812–820 (2012)
30. H.M. Muhmond, *On the Inoculation and Graphite Morphologies of Cast Iron*. Doctoral Thesis, The Royal Institute of Technology (2014)
31. A.R. KianiRashid, D.V. Edmonds, Graphite phase formation in Al-alloyed ductile irons. IJE Trans. B Appl. **15**(3), 261–272 (2002)
32. A. Shayesteh-Zeraati, H. Naser-Zoshki, A.R. Kiani-Rashid, Microstructural and mechanical properties (hardness) investigations of Al-alloyed ductile iron Al-alloyed ductile cast iron. J. Alloys Compd. **500**, 129–133 (2010)